Microfluidic Multifunctional Probe Array Dielectrophoretic Force Spectroscopy with Wide Loading Rates

In Soo Park,[†] Kilho Eom,[†] Jongsang Son,[†] Woo-Jin Chang,[‡] Kidong Park,[§] Taeyun Kwon,[†] Dae Sung Yoon,[†] Rashid Bashir,[*,§] and Sang Woo Lee[*,†]

[†]Department of Biomedical Engineering, Yonsei University, Won-Ju, 220-710, Korea, [‡]Department of Mechanical Engineering, Universiyt of Wisconsin—Milwaukee, Milwaukee, Wisconsin 53201, United States, and [§]Department of Electrical and Computer Engineering, Department of Bioengineering, and Micro and Nanotechnology Laboratory, University of Illinois at Urbana—Champaign, Illinois 61801, United States

ABSTRACT

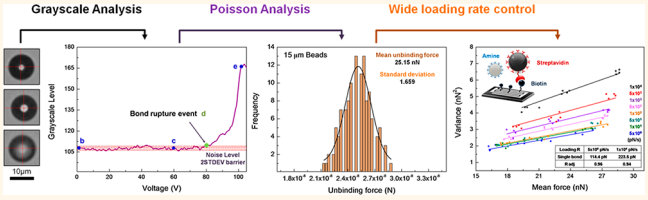

The simultaneous investigation of a large number of events with different types of intermolecular interactions, from nonequilibrium high-force pulling assays to quasi-equilibrium unbinding events in the same environment, can be very important for fully understanding intermolecular bond-rupture mechanisms. Here, we describe a novel dielectrophoretic force spectroscopy technique that utilizes microsized beads as multifunctional probes for parallel measurement of intermolecular forces with an extremely wide range of force rate (10^{-4} to 10^{4} pN/s) inside a microfluidic device. In our experiments, various forces, which broadly form the basis of all molecular interactions, were measured across a range of force loading rates by multifunctional probes of various diameters with a throughput of over 600 events per mm^2, simultaneously and in the same environment. Furthermore, the individual bond-rupture forces, the parameters for the characterization of entire energy landscapes, and the effective stiffness of the force spectroscopy were determined on the basis of the measured results. This method of determining intermolecular forces could be very useful for the precise and simultaneous examination of various molecular interactions, as it can be easily and cost-effectively implemented within a microfluidic device for a range of applications including immunoassays, molecular mechanics, chemical and biological screening, and mechanobiology.

KEYWORDS: dielectrophoresis · force spectroscopy · intermolecular interactions · microfluidic device · quasi-equilibrium unbinding events · high-force pulling assay

The characterization of biochemical bonds in biological processes, from cell adhesion to protein/RNA unfolding, requires the measurements of a large number of individual events for obtaining statistically reliable data to draw specific conclusions.[1−3] Moreover, since some biological processes rely on the interplay of different types of intermolecular bonds, generating statistically reliable data with different intermolecular forces simultaneously and in the same environments is also an important issue. Studies involving measurements of intermolecular forces have also found that the forces required for rupturing the bonds can vary significantly when estimated using different loading rates.[4] For instance, in an experiment probing the viscoelasticity of titin, the force required for unfolding of individual titin domains was estimated to be about 10 pN at a loading rate of about 10^{-2} pN/s.[5] On the other hand, in an AFM pulling experiment, the force required to unfold individual titin domains was measured to be about 200 pN at a loading rate of about 100 pN/s.[6] In addition, force-driven bond ruptures observed with a wide range of loading rates have been used as a model system to validate the physical theories on phase transition. It is shown that the kinetics of the chemical reaction driven by a mechanical force is strongly dependent on the loading rate (r_f) in such a way that the force required for the reaction is proportional to $\log(r_f)$ at low loading rate and $[\log(r_f)]^{3/2}$ at a high loading rate.[7,8] Force-driven bond-rupture experiments have also been used to verify nonequilibrium dynamics theories such as Jarzynski's theory and Crooks' theory.[9,10] Furthermore, the intermolecular bond rupture depends on not only the loading rate but also the "effective stiffness" (defined as $\Delta F/\Delta x$) of the force probe or the method used for the force measurement.[11] Hence, the control of an extremely wide range of loading rate within a force spectroscopy assay can be very desirable, from quasi-equilibrium intermolecular unbinding events that require extremely low loading rates to

* Address correspondence to yusuklee@yonsei.ac.kr; rbashir@illinois.edu.

Received for review May 18, 2012 and accepted August 31, 2012.

Published online September 11, 2012
10.1021/nn302202t

nonequilibrium bond-rupture assays that require high loading rates.

Current force spectroscopy methods such as atomic force microscopy (AFM), laser optical tweezers, and biomembrane force probes can handle individual single molecules (*e.g.*, AFM), perform measurement of biological samples under near-physiological conditions (*e.g.*, AFM or biomembrane force probe), and measure molecular motions by manipulating sub-nanometer- to micrometer-sized particles with sub-nanometer accuracy (*e.g.*, optical tweezers).[12−17] However, those techniques have only been applied for the measurement of a single to a few binding events at a time. In general, the loading rates of AFM, optical tweezers, and biomembrane force probes are limited to the ranges $\sim 10-10^7$, $\sim 10^{-1}-10^2$, and $\sim 10^{-1}-10^4$ pN/s, respectively, and none can reach a very low loading rate ($<10^{-2}$ pN/s) due to the low-frequency drift from mechanical or optical components. Shear force spectroscopy can measure many biological binding events simultaneously.[18−21] Moreover, recent papers reported that microfluidic force in combination with dielectrophoretic (DEP) force can be used for the detachment of biomolecular interactions with very accurate resolution (~piconewton range); however the loading rate was not explored in this study.[20,21] Magnetic tweezers have recently been suggested as a force spectroscopy method enabling the parallel measurements at low loading rates ($\sim 10^{-3}-10^0$ pN/s).[22] However, the presence of nonuniform magnetic fields and a magnetic field gradient at different locations on the substrate can lead to measurement uncertainty.[22] Even though electromagnetic tweezers can allow three-dimensional manipulation, the implementation can be complicated. Realization of the large magnetic field and gradients require high-current electromagnets that can produce substantial heating. Additional challenges include fabricating tweezers with multiple magnetic poles for the generation of repulsive and attractive forces while ensuring minimal pole interference and fabrication of small, closely spaced pole pieces that cannot realize the constant-force benefit of this approach.[23,24]

Dielectrophoretic tweezers can be used to measure intermolecular forces and provide many advantages over currently available approaches.[25,26] The technology is inexpensive, easy to implement with simple on-chip interdigitated (IDT) electrodes used to generate the forces, and ideally suited for integration inside a microfluidic device as compared to other approaches.[26,27] The technology can achieve precise local control of the electric fields and corresponding DEP forces generated using the IDT electrodes, since the DEP force scales as the second power of the dimension of IDT structures, *versus* the fourth power of the dimension of the microcoils in the case of magnetic tweezers.[28] Moreover, our multifunctional probe array DEP force spectroscopic technique employs hundreds of functionalized polystyrene beads at an interrogation density of about 600 events/mm^2, where each bead acts as a probe inside the microfluidic device with fabricated IDT electrodes. It offers parallel measurements of interactions between different molecules simultaneously and under the same conditions. The technique can also provide a wider dynamic range of applied force and loading rates ($\sim 10^{-4}-10^4$ pN/s) as compared to any other approach.

In this study, we examined various forces that broadly form the basis of all molecular interactions in order to establish that our approach can be used for a wide range of applications. First, the method was utilized for the investigation of hydrogen bond interactions using carboxyl-terminated molecules on beads and surfaces and the ionic interactions between carboxyl-terminated and amino-terminated molecules. Then, we also measured specific ligand−receptor interactions using the well-known streptavidin−biotin model system, and nonspecific interactions were examined using the case of amino-terminated and biotin-terminated molecules. The technique was also used to simultaneously examine two different ligand−receptor interactions (streptavidin−biotin and avidin−biotin) with loading rates ranging from 10^0 to 10^4 pN/s. Lastly, in the very low force loading region ($\sim 10^{-4}-10^0$ pN/s), attraction forces in the range of a few pico-Newtons were measured between two negatively charged carboxyl-terminated molecules.

RESULTS

DEP Force Spectroscopy. Carboxyl-functionalized beads of 10 μm diameter were used as probes to measure the intermolecular forces. Figure 1a shows the schematic diagram of the measurement system. Optical images (Figures 1b−e) were taken sequentially as the magnitude of the ac voltage (at a frequency of 10 MHz) was increased. The IDT electrodes were covered by an oxide layer functionalized with a succinic anhydride layer, and the beads were suspended in deionized (DI) water at pH 4. Figure 1b shows the randomly distributed beads on the functionalized oxide surface without application of the ac voltage. It can be safely assumed that a hydrogen bond has been established between each bead and the functionalized surface.[26] As shown in Figure 1c−e, by increasing the magnitude of the negative DEP force generated by the ac voltage across the IDT electrodes, the beads moved toward the middle of each IDT electrode (where the electric field gradient was lowest and directed vertically) and were eventually pulled away from the surface. In general, a bead attached on a surface by an intermolecular bond does not move upward from the surface until the intermolecular bond with the surface is completely ruptured due to the applied DEP force. Since the applied force corresponding to the bead movement is correlated by optical imaging to the movement of the beads, the unbinding force can be determined. Previous reports have

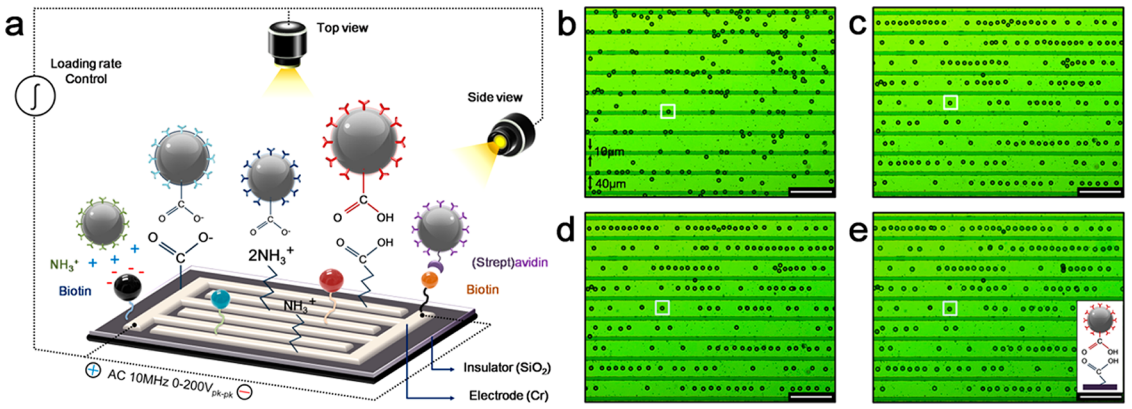

Figure 1. (a) Schematic diagram for the measurement system. (b–e) Optical images of 10 μm polystyrene beads on the electrode covered by a succinic anhydride-functionalized oxide layer with the application of voltages of (b) 0 V, (c) 60 V, (d) 80 V, and (e) 100 V.

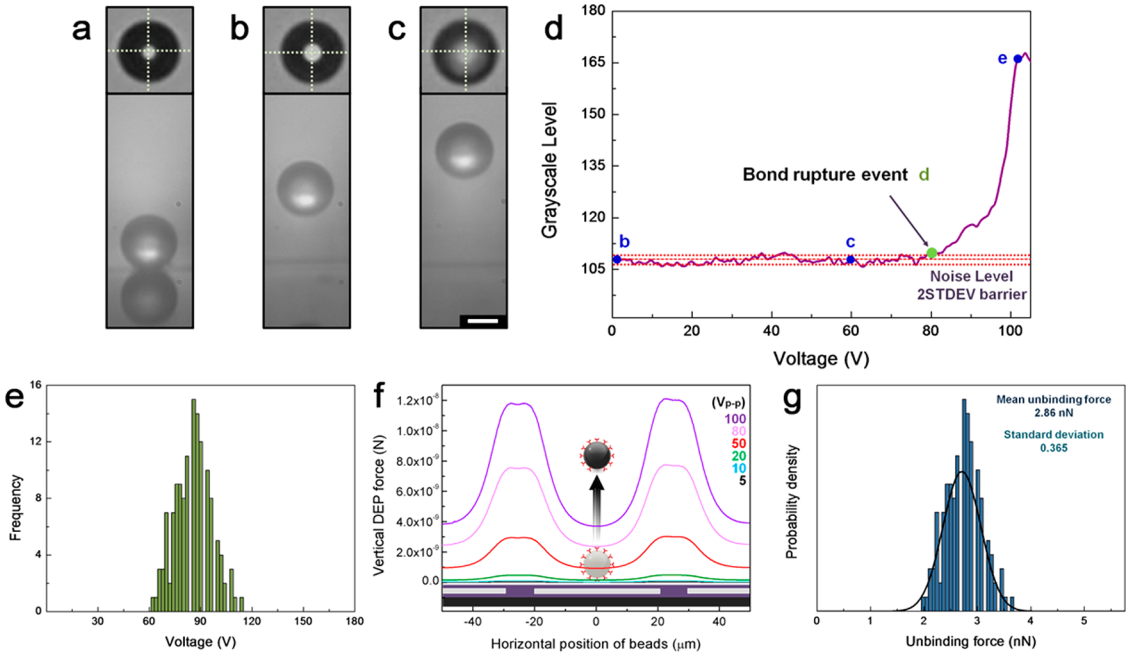

Figure 2. (a–c) Top view images with different grayscales (top) and side view images corresponding to the top view images, respectively (bottom); scale bar is 5 μm: (a) 0 V, (b) 1.5 V, (c) 3 V. (d) Grayscale and height variation graph as a function of applied voltage. (e) Histogram graph representing the number of hydrogen bond unbinding events as a function of applied voltage. (f) Simluated vertical DEP force at 6 μm height above the electrode as increasing voltage was applied. (g) Histogram and Gaussian fitting graphs as a function of unbinding force that ruptures the hydrogen bond.

determined the initial distance variation using fluorescence or optical defocusing to estimate the unbinding forces.[22,25,26] However, since those methods rely on manual determination of the distance variation, the estimated values could be unreliable. Our current work developed a "grayscale variation method" to overcome the manual estimation and the potential reliability issues inherent in previously used methods. Figure 2a–c show the top and side view images of a bead under the application of 0, 1.5, and 3 V. The grayscale value from the top view images is clearly distinguished as the bead moves upward. Using these grayscale differences, a Matlab code was used to automatically quantify the grayscale variation. Moreover, in this method the noise level, defined by the fluctuation in the grayscale value, can be established by the experiments and statistics to determine when a rupture of an intermolecular bond occurs (see Supporting Information A).

Figure 2d is an example of the grayscale variation corresponding to the distance variation of the bead inside the small box shown in Figure 1b–e. As shown in Figure 2d, when the hydrogen bond between the bead and surface is not completely ruptured by the applied DEP force (*e.g.*, where bead is visible at the surface at 0 V in Figure 1b and when the bead is located at the center of the IDT electrode at 60 V in Figure 1c), the grayscale value stays within the noise level, or the grayscale value that is outside the noise level returns to

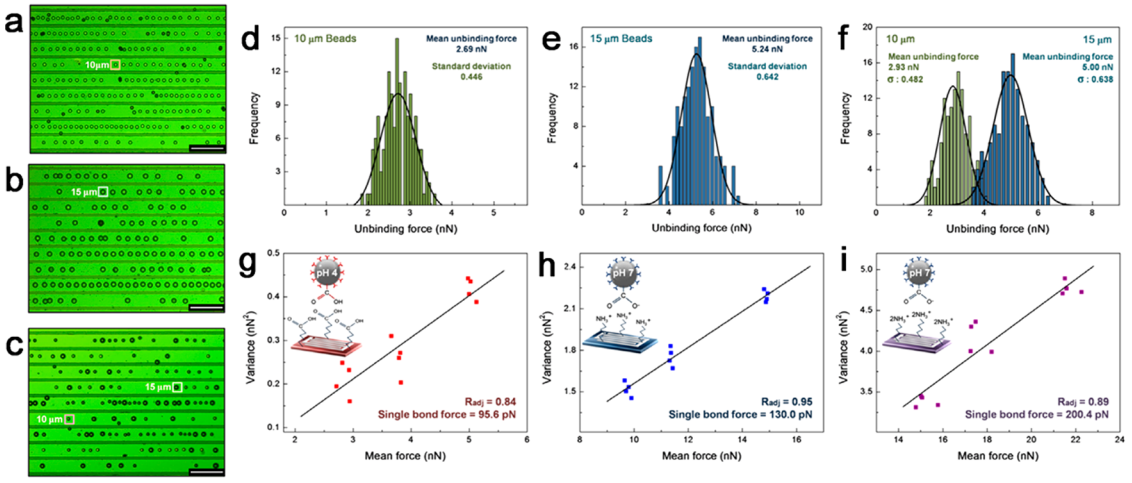

Figure 3. (a−c) Optical images of carboxyl-terminated polystyrene beads located on the center of the electrodes covered by the succinic anhydride-functionalized oxide surface: (a) 10 μm beads, (b) 15 μm beads, (c) 10 and 15 μm beads. (d−f) Histogram and Gaussian fitting graphs as a function of unbinding force that ruptures the hydrogen bond: (d) 10 μm beads, (e) 15 μm beads, (f) 10 and 15 μm beads. (g−i) Variance *vs* mean graphs to calculate an individual bond-rupture force for (g) the hydrogen interaction between carboxyl-terminated beads and succinic anhydride-functionalized oxide surface, (h) the ionic interaction between the carboxyl-terminated beads and APTES-functionalized oxide surface, and (i) the ionic interaction between the carboxyl-terminated beads and L-lysine-functionalized oxide surface.

within the noise level as the applied voltage increases. When the hydrogen bond between the bead and the surface ruptures completely, the grayscale value exceeds the noise level (*e.g.*, where the bead separates from the surface at 80 V in Figure 1d) and continues to increase as the applied voltage increases (*e.g.*, where the bead further separates from the surface at 100 V in Figure 1e). On the basis of these observations, the unbinding voltage is defined as the voltage corresponding to the lowest grayscale value at which the grayscale value exceeds the noise level and continues to increase (*e.g.*, 80 V in Figure 1d among the voltages at which images in Figure 1b−e were recorded). This unbinding voltage histogram (Figure 2e) can be used to determine the actual force of the interaction by calculating the DEP force on the bead using a model described earlier.[25,26] Figure 2f is an example of simulated vertical DEP force at 6 μm height above the electrode as a function of applied voltage. Using the simulation, the unbinding force histogram corresponding to Figure 2e was obtained as shown in Figure 2g. The mean unbinding force for a hydrogen bond between two nonionized carboxyl-terminated groups is 2.86 $\pm$ 0.36 nN. While this value is in good agreement with earlier reports, unlike any other report, it is measured by obtaining hundreds of experimental values in parallel in a fraction of the time as compared to the scanning probe approaches that provide a single value per measurement.[29−31]

Multiple Probe Array DEP Force Spectroscopy with Different Probe Diameters. The technique allows the use of multiple, different diameter probes that obtain large ensemble measurements of different numbers of intermolecular bonds formed with the probes of different diameter, simultaneously and in the same environment. We validate the DEP force spectroscopy approach by first employing multiple probes with the same diameter and then employing multiple probes with different diameters and comparing these results for hydrogen-bonding interactions. Using many carboxyl-terminated beads with the same diameter of either 10 or 15 μm (Figure 3a,b) or the different diameters of 10 and 15 μm (Figure 3c), located on a succinic anhydride-functionalized oxide surface, the upward movement of the beads was determined as the voltage was increased in order to obtain the histograms of the unbinding forces required to break the hydrogen bond between the beads and the surface (Figure 3d−f). The unbinding force calculated by this approach was 2.69 $\pm$ 0.45 nN (for 10 μm diameter beads) and 5.24 $\pm$ 0.64 nN (for 15 μm diameter beads). The unbinding forces calculated by the approach employing multiple, different diameter probes were 2.93 $\pm$ 0.48 and 5.00 $\pm$ 0.64 nN (10 and 15 μm multiple probes together). We also used multiple beads consisting of only 12 μm beads or a combination of 12 and 15 μm. The mean forces and standard deviations recorded by multiple beads of the same or multiple diameters are summarized in Table S1. Using these values, the individual bond-rupture force of the hydrogen bond was calculated by applying the Poisson distribution statistical method to the mean and variance of force obtained from the unbinding measurement data recorded by multiple probes with different diameters.[32,33] By applying this statistical method to the data in Figure 3g, the individual bond-rupture force of the hydrogen bond is calculated to be 95.6 pN with a coefficient of determination of R = 0.84 (see Supporting Information B). This value is in agreement with previous studies, but can be obtained in a fraction of the time needed to perform the serial measurements.[34,35]

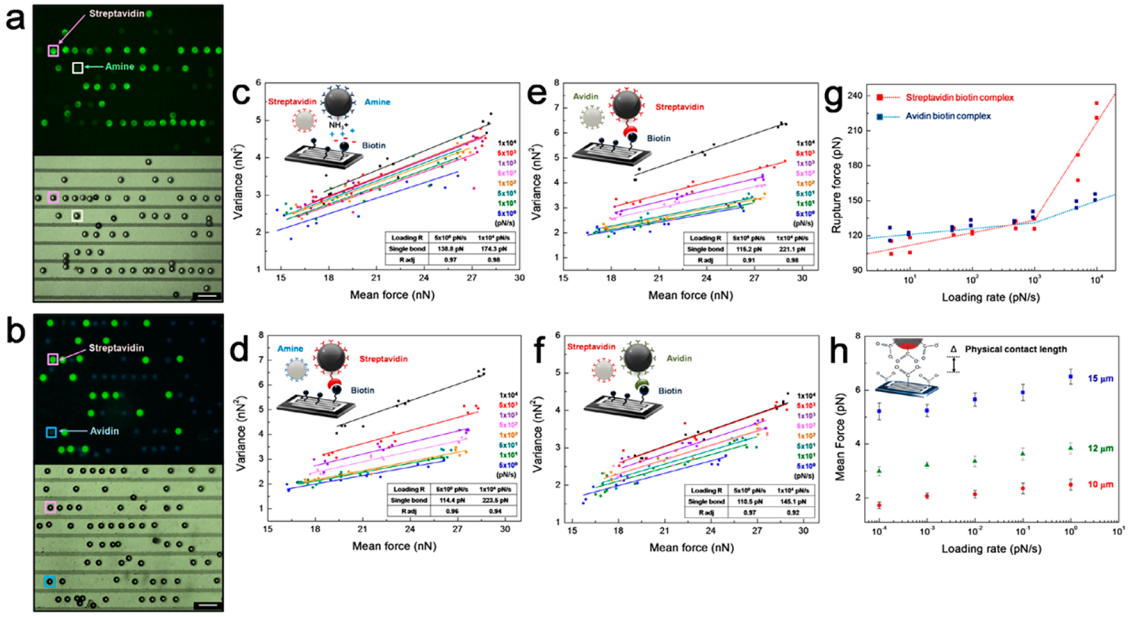

Figure 4. (a, b) Optical images of 15 μm functionalized beads located on the center of the electrodes covered by the biotin-functionalized oxide surface: (a) amino-terminated polystyrene beads and streptavidin-terminated beads; (b) avidin-terminated polystyrene beads and streptavidin-terminated beads. (c, d) Variance *vs* mean force graphs to calculate an individual bond-rupture force as the force loading rate is varied to effect (c) ionic interaction between amino-terminated beads and biotin-functionalized oxide surface and (d) ligand−receptor interaction between the streptavidin-terminated beads and biotin-functionalized oxide surface. (e, f) Variance *vs* mean force graphs to calculate an individual bond-rupture force for two different ligands as the force loading rate is varied to effect (e) streptavidin−biotin interaction and (f) avidin−biotin interaction. Each inset of (c)−(f) describes the individual bond-rupture forces at the lowest and highest force loading rates. (g) Individual rupture force *vs* the force loading rate to calculate the energy landscape of the streptavidin−biotin and avidin−biotin interactions. (h) Mean force *vs* the force loading rate for the van der Waals interaction between the carboxyl-terminated functionalized beads and the succinic anhydride-functionalized oxide surface.

We next investigated the ionic interactions between the differently sized carboxyl-coated beads and positively charged oxide surface functionalized by 3-aminopropyltriethoxysilane (APTES) or L-lysine using the methodology described above. The acid dissociation constants (p*K*'s) of the amino-terminated molecule in the tail group of the APTES-functionalized surface, the amino-terminated molecule in the tail group of the L-lysine-functionalized surface, and the carboxyl-terminated molecule in the tail group of the beads are 11, >9, and <5, respectively.[36−38] Hence, at pH 7, it is expected that the positive charges on the amino-terminated molecules and the negative charges on the carboxyl-terminated molecules will result in an ionic interaction. The mean bond-rupture force and standard deviation of the ionic interactions between the carboxyl group and APTES surface or L-lysine surface in DI water at pH 7 was measured, and results are shown in Table S2. Moreover, the individual bond-rupture forces are extracted to be 130.0 pN for the carboxyl group- and APTES-functionalized surface and 200.4 pN for the carboxyl group- and L-lysine-functionalized surface, as shown in Figure 3h,i.

Multifunctional Probe Array DEP Force Spectroscopy with Extremely Wide Loading Rate. Nonspecific interactions occur in biological assays and need to be minimized or eliminated. Quantitative characterization of nonspecific and specific interactions simultaneously in the same environment can be very useful in designing immunoassays and determining conditions to achieve specific capture in microfluidics.[39,40] In our experiment, a combination of 15 μm diameter amino-terminated beads and 15 μm streptavidin-terminated beads (which also had a fluorescent label) were introduced on electrodes covered by a biotin-functionalized oxide surface (Figure 4a). The beads arranged on the center of the electrode were imaged as the loading rate was increased from 1 pN/s to 10^4 pN/s (Supporting Information C). The variance as a function of the mean force between the amino-terminated beads and streptavidin-terminated beads with 10, 12, and 15 μm diameters and the biotin-functionalized oxide surface in a solution of DI water at pH 7 under various loading rates was plotted as shown in Figures 4c and d. The figure insets describe the individual bond-rupture force of an ionic interaction (a nonspecific interaction) between the positively charged amino-terminated beads and the negatively charged biotin-terminated functionalized surface and a ligand−receptor interaction (a specific interaction) between the streptavidin-terminated beads and the biotin-functionalized surface at the lowest and highest loading rates.[41] The individual bond-rupture forces of the ionic interaction and ligand−receptor interaction vary from 138.8 to 174.3 pN and from 114.3 to 224.4 pN, respectively.

We also investigated the individual bond-rupture force between streptavidin–biotin and avidin–biotin with a wide loading rate ($\sim 1 - 10^4$ pN/s). Figure 4b shows the combination of 15 μm streptavidin- and avidin-functionalized beads, which were used for the measurement of the force between two different ligands, located on the center of the electrode covered by the biotin-functionalized oxide surface. The variances of the streptavidin–biotin and avidin–biotin interactions measured using 10, 12, and 15 μm streptavidin-terminated beads and avidin-terminated beads were plotted as a function of mean force in Figure 4e and f. Figure 4g shows the individual bond-rupture force as a function of the loading rate extracted from Figure 4e and f. A low loading rate, $\sim 10^{-4} - 1$ pN/s, was used to examine the intermolecular force between the varying sized carboxyl-terminated beads and the succinic anhydride-functionalized surface in DI water at pH 7. Figure 4h shows the mean force as a function of the DEP force loading rate and that an intermolecular attractive force in the pN range exists between the beads and the surface. Especially, this wide range of lowest loading rate ($\sim 10^{-4}$ pN/s) has not been reported before by linear force ramps.[22,23]

DISCUSSION

In this work, the measured mean forces, such as hydrogen bonding using 10 μm carboxyl-terminated beads, and the individual bond-rupture forces of hydrogen bonds between two neutralized carboxyl groups (Figure 3d and g) are in good agreement with previous reports.[25−27] The minor discrepancies between our experimental results and those of previous reports can be explained by the differences between the contact area of the bead employed in our studies and the contact area of the probe tips used in the previous experiments. For instance, in our data (Exp 2, Table S1), the measured mean binding forces of a hydrogen bond are about 2.86 nN (for 10 μm diameter beads), 3.71 nN (for 12 μm diameter), and 5.09 nN (for 15 μm diameter). The individual bond-rupture force of a hydrogen bond between two neutralized carboxyl groups, as shown in Figure 3g, obtained by our method is also slightly different compared with the result in the earlier reports.[35,36] These minor discrepancies could be from the variation in the surface charge density of the functionalized group in the contact area. It should also be noted that the individual ionic bond-rupture forces using the APTES-functionalized surface are clearly distinguishable from that of the L-lysine-functionalized surface in our method. This difference can be explained by the chemical components of the two molecules. There is one amino-terminated molecule in the tail group of the APTES-functionalized surface and two in that of the L-lysine-functionalized surface.[37,38] Therefore, the individual ionic bond-rupture forces of the L-lysine-functionalized surface are greater than that of the ATPES-functionalized surface. Such precise and rapid discrimination of the forces between these molecules in a large array of beads opens the possibility of measuring the biological or chemical interactions in a very high-throughput manner.

The ability to investigate molecular bond rupture using multifunctional probes with an extremely wide range of loading rates could be used to characterize biological processes easily and rapidly and could also provide the necessary tools for investigating a bond-rupture mechanism. In our experiments, specific (streptavidin–biotin) and nonspecific (NH_3^+–biotin) interactions and two different ligand–receptor interactions (streptavidin–biotin and avidin–biotin) were measured simultaneously in the same environment, and the different individual bond-rupture forces associated with the measured values are clearly determined, as shown in Figure 4c–f. Moreover, the bond-rupture force range from bound state to unbounded state could depend on which type of chemical bond is involved in the molecular interaction (Table S3). The result from Figure 4g and h, which are obtained by the accessibility of both quasi-equilibrium (extremely low loading rate) and nonequilibrium (high loading rate) processes of our method, can be regarded as a model system for the verification of physical theories in phase transitions. For instance, assuming a linear relationship between the rupture force and the logarithm of the force loading rate from the Bell model, $f^* = (k_BT/x_\beta) \ln((x_\beta r_f)/(k^0 k_B T))$, with the data in Figure 4g, x_β, the dissociation rate in terms of an energy barrier width in the entire energy landscape, can be calculated, where f^*, k_B, T, r_f, and k^0 are the binding force, Boltzmann's constant, absolute temperature, loading rate, and the dissociation rate constant in the absence of applied force, respectively.[42,43] From 1 pN/s to 10^3 pN/s, x_β for the streptavidin–biotin and avidin–biotin interactions are 0.50 and 0.54 nm, respectively, and they become 0.15 and 0.30 nm when the loading is increased from 10^3 pN/s to 10^4 pN/s. In the low loading rate case, the rupture forces of the streptavidin–biotin interaction are close to those of the avidin–biotin interactions, but the rupture forces between the two different ligands are still clearly distinguishable. The calculated x_β values and the characteristics of the individual bond-rupture rate under various loading rate are in good agreement with previous results.[42,43] In addition, the unbinding forces, as shown in Figure 4h, are found to saturate at loading rates less than 10^{-2} pN/s, which implies that unbinding likely occurs during a quasi-equilibrium condition, as predicted by Bell's model.

An interesting observation in Figure 4h is to measure the intermolecular attractive force even though there are negatively charged molecules between the carboxyl-terminated beads and succinic anhydride-functionalized oxide surface. In order to

explain this phenomenon, the intermolecular attractive forces could be augmented by hydrophobic interaction, gravitational force, and van der Waals force in our measurement approach. Hydrophobic interactions can be ignored because while the bead might be hydrophobic, the surface is hydrophilic. The effects of gravity can also be ignored (Supporting Information D). Lastly, the van der Waals force between a sphere and half-plane can be analyzed by $F_{\text{Van-der-Waals}} = Ad/12\Delta^2$, where A ($\approx (3/4)k_BT$) is the Hamaker constant, d is the particle diameter, and Δ is the physical contact length.[44,45] By associating the mean unbinding forces in Figure 4h with the van der Waals' formula mentioned above, the physical contact length (Δ) can be calculated to be from about 24 to 38 nm as the loading rate decreases. This range of separated distance closely matches the distance between the 9.8 μm polystyrene beads and a fluorocarbon or PEG surface in the region of low loading rate (10^{-2}–10^{-1} pN/s).[22] The large separation distance in our experimental system can be explained by an electrical repulsion between the negatively charged carboxyl-terminated beads and the negatively charged succinic anhydride-functionalized surface in DI water at pH 7. It can also be observed from Figure 4h that the attractive force increases with increasing bead diameter, which follows the characteristics of the van der Waals force described by the formula above. Taken in aggregate, the above observations suggest that the attractive force analyzed in Figure 4h could be the van der Waals force.

It has also been recently reported that the "effective constant" (defined as $\Delta F/\Delta x$) of the force probe or the method used for the force measurement is a critical factor to estimate the bond-rupture force.[11] Specifically, for an unbinding measurement of the avidin–biotin complex at a loading rate of $\sim 10^3$ pN/s, the bond-rupture force measured by the biomembrane force probe is obtained as ~60 pN, whereas the bond-rupture force estimated by our DEP probe is ~135 pN (Table S3).[43] In order to understand the dependency of the force measurement on the stiffness of the method, we have theoretically considered theory using a linear-cubic potential in the free energy landscape (Supporting Information E). As shown in Figure S3, the force required for such an unbinding experiment is governed by both loading rate and the stiffness of the force probe. In particular, at a loading rate of $\sim 10^3$ pN/s, the unbinding force measured by a probe with a stiffness of 10^2 pN/nm (corresponding to the stiffness of our DEP probe) is predicted as ~130 pN, while the unbinding force measured by a biomembrane force probe with a stiffness of $\ll 1$ pN/nm is anticipated as ~80 pN. These results clearly show that stiffness of the force probe in the measurement of unbinding force (or bond-rupture forces) is important, and our method allows the measurement over a wide loading range with the same effective stiffness.

CONCLUSION

In conclusion, our DEP force spectroscopy enables the high-throughput measurement of molecular bond rupture over a wide range of loading rate and allows easy implementation within microfluidic devices. The accessibility of a loading rate ranging from quasi-equilibrium to nonequilibrium states can enhance the understanding of the fundamental mechanisms behind bond rupture. Using the experimentally obtained unbinding voltages over a wide range of loading rate, the mean unbinding forces and their standard deviation were determined for various biochemical molecular interactions. Furthermore, the results were used to determine the individual bond-rupture force parameters for the characterization of entire energy landscapes and the effective stiffness of the force spectroscopy. This new method of determining intermolecular forces could be very useful for a range of applications underpinning mechanism such as cellular surface adhesion, enzymatic activity, or molecular recognition, as it can be easily and cost effectively implemented within a microfluidic device.

METHODS

Micro-Chip Fabrication. A 0.2 μm thick chromium interdigitated electrode array pattern was created on an oxidized silicon wafer using the thermal evaporator technique and lift-off process, where each electrode line was 40 μm wide and 10 μm apart. The metal electrodes were covered by a 0.8 μm thick plasma-enhanced chemical vapor deposited silicon dioxide with a TEOS (tetraethylorthosilicate) source. Then, the contact pads to apply ac voltage into the array were opened by a wet etching process.

Functionalized Beads. Functionalized polystyrene beads (carboxyl-terminated, amino-terminated, streptavidin-terminated, and Avidin-terminated beads) used in the experiments were purchased from Kisker Biotech GmbH & Co.KG. For the experiments herein, the original stock solution was diluted by DI water, and the concentration of beads in the diluted solution was $\sim 5 \times 10^5$ particles/mL (Supporting Information F).

Functionalized Surfaces. Each functionalized surface such as the carboxyl-terminated oxide surface by succinic anhydride (Sigma, 23960), amino-terminated oxide surface by 3-aminopropyltriethoxysilane (APTES, Sigma, A3648), amino-terminated oxide surface layer by L-lysine (Sigma, L5501), and biotin-terminated oxide surface by biotinylated bovine serum albumin (Sigma, A8549) was prepared using the modified Stöber method (Supporting Information G).

Experimental Setup. The silicon dioxide surface inside the microchip was functionalized using different molecules. A PDMS (polydimethylsiloxane) layer was then used to form an open reservoir over the chip. Functionalized polystyrene beads suspended in a DI water solution were introduced onto the chip. Subsequently, a glass slide was used to cover the top of the PDMS reservoir. In order to apply less than 12 $V_{\text{peak-to-peak}}$ into the electrode, a sinusoidal signal at 10 MHz from a function generator (Agilent 33250 or National Instrument PXI/PCI-5421) was applied

using micromanipulator probes to the chip. For the high-voltage application, the sinusoidal signal at 10 MHz was applied to the chip using the amplifier (Amplifier Research 150 L, Electronics & Innovation A150) that was already connected to the function generator. Upon applying the sinusoidal signal with various peak values and loading rates (Supporting Information C), the movement of the beads was observed and recorded under top-view and side-view microscopes using a CCD camera. The temperature variation on the silicon oxide surface was also measured using a thermocouple (HUATO, HE701) while keeping the same experimental conditions. The measurement and experimental results are presented in Supporting Information H.

Method for Converting Applied Voltage to Dielectrophoretic Force. The DEP force is given by

$$\vec{F}_{\text{total}} = \sum_{0}^{\infty} -\nabla U_n$$

$$U_n = -\frac{2\pi\varepsilon_m K_n r^{(2n+1)}}{(2n+1)!!} \sum_{i+j+k=n} \frac{1}{i!j!k!}\left[\frac{\partial^n \Phi}{\partial x^i \partial y^j \partial z^k}\right]^2$$

$$K_n = \frac{n(2n+1)(\tilde{\varepsilon}_p - \tilde{\varepsilon}_m)}{n\tilde{\varepsilon}_p + (n+1)\tilde{\varepsilon}_m} \quad (1)$$

where n is the force order, Φ refers to the electrostatic potential of the external electric field, and K_n is the nth-order Clausis–Mossotti factor.[25,26] Based on this equation, a Matlab (R12, Mathworks) code was developed for calculating the total DEP force. The electrical-field profiles for the IDT electrodes used for the experiment, when the ac signal with 1 $V_{\text{peak-to-peak}}$ and 10 MHz was applied to the electrodes, were generated from a finite element program (version 5.7, ANSYS Inc.) with grid spacing of 0.2 μm. The experimental parameters and the generated electric-field data were used as inputs for the Matlab code. As a result, the dielectrophoretic force can be calculated as a function of the applied voltage (Supporting Information I). The variation of the voltage to break an intermolecular bond *versus* the oxide thickness on the electrodes is also examined in Supporting Information J.

Conflict of Interest: The authors declare no competing financial interest.

Acknowledgment. This work was supported in part by the Korean Ministry of Education and Science (Grant Nos. NRF-2010-0026223, NRF-2010-0027238, NRF-2010-0013619, and NRF-2009-0068841) and support from University of Illinois at Urbana–Champaign.

Supporting Information Available: Supplementary methods for analyzing grayscale variation due to voltage application to the IDT electrode, for calculating an individual rupture force using Poisson statistics, and for applying force loading rate to the system are described in Supporting Information A, B, and C. Gravitational force on the beads in our system and theoretical analysis of the effect of the stiffness of force spectroscopy are in Supporting Information D and E, respectively. Supporting Information F and G explain the methods for preparing the functionalized beads and functionalized surface. The investigation of temperature variation on the oxide surface as the applied voltage is varied is presented in Supporting Information H. Supporting Information I and J describe the method to convert applied voltage to dielectrophoretic force, and the variation of applied voltage for keeping the DEP force at a certain position from the oxide surface while varying the thickness of the oxide, respectively. Lastly, the supplementary tables, which summarize the measured results and the parameters used to calculate the DEP force, are also presented. This material is available free of charge *via* the Internet at http://pubs.acs.org.

REFERENCES AND NOTES

1. McEver, R. P.; Zhu, C. Rolling Cell Adhesion. *Annu. Rev. Cell. Dev. Biol.* **2010**, *26*, 363–396.
2. Bustamante, C.; Chemla, Y. R.; Forde, N. R.; Ishaky, D. Mechanical Processes in Biochemistry. *Annu. Rev. Biochem.* **2004**, *73*, 705–748.
3. Borgia, A.; Williams, P. M.; Clarke, J. Single-Molecule Studies of Protein Folding. *Annu. Rev. Biochem.* **2008**, *77*, 101–125.
4. Eom, K.; Makarov, D. E.; Rodin, G. J. Theoretical Studies of the Kinetics of Mechanical Unfolding Cross-Linked Polymer Chains and Their Implications for Single-Molecule Pulling Experiments. *Phys. Rev. E* **2005**, *71*, 0210904.
5. Minajeva, A.; Kulke, M.; Fernandez, J. M.; Linke, W. A. Unfolding of Titin Domains Explains the Viscoelastic Behavior of Skeletal Myofibrils. *Biophys. J.* **2001**, *80*, 1442–1451.
6. Rief, M.; Gautel, M.; Oesterhelt, F.; Fernandez, J. M.; Gaub, H. E. Reversible Unfolding of Individual Titin Immunoglobulin Domains by AFM. *Science* **1997**, *276*, 1109–1112.
7. Bell, G. I. Models for the Specific Adhesion of Cells to Cell. *Science* **1978**, *200*, 618–627.
8. Garg, A. Escape-Field Distribution for Escape from Metastable Potential Well Subject to a Steadily Increasing Bias Field. *Phys. Rev. B* **1995**, *51*, 251–341.
9. Liphardt, J.; Dumon, S.; Smith, S. B.; Tinoco, I., Jr.; Bustamante, C. Equilibrium Information from Nonequilibrium Measurements in an Experimental Test of Jarzynski's Equality. *Science* **2002**, *296*, 1832–1835.
10. Collin, D.; Ritort, F.; Jarzynski, C.; Smith, S. B.; Trinoco, I., Jr.; Bustamante, C. Verification of the Crooks Fluctuation Theorem and Recovery of RNA Folding Free Energies. *Nature* **2005**, *437*, 231–234.
11. Martra, A.; Arya, G. Model Accounting for the Effects of Pulling-Device Stiffness in the Analyses of Single-Molecule Force Measurements. *Phys. Rev. Lett.* **2010**, *1004*, 108301.
12. Lee, C. K.; Wang, Y. M.; Huang, L. S.; Lin, S. Atomic Force Microscopy: Determination of Unbinding Force, Off Rate and Energy Barrier for Protein-Ligand Interaction. *Micron* **2007**, *38*, 446–461.
13. Bustamante, C.; Rivetti, C.; Keller, D. J. Scanning Force Microscopy Under Aqueous Solutions. *Curr. Opin. Struct. Biol.* **1997**, *7*, 709–716.
14. Shiroguchi, K.; Kinosita, K., Jr. Myosin V Walks by Lever Action and Brownian Motion. *Science* **2007**, *316*, 1208–1212.
15. Moffitt, J. R.; Chemla, Y. R.; Izhaky, D.; Bustamante, C. Differential Detection of Dual Traps Improves the Spatial Resolution Optical Tweezers. *Proc. Natl. Acad. Sci. U. S. A.* **2006**, *103*, 9006–9011.
16. Evans, E. Looking inside Molecular Bonds at Biological Interfaces with Dynamic Force Spectroscopy. *Biophys. Chem.* **1995**, *82*, 83–97.
17. Evans, E.; Ritchie, K.; Merkel, R. Sensitive Force Technique to Probe Molecular Adhesion and Structural Linkages at Biological Interface. *Biophys. J.* **1995**, *68*, 2580–2587.
18. Cozens-Roberts, C.; Lauffenburger, D. A.; Quin, J. A. Receptor-Mediated Cell Attachment and Detachment Kinetics: I. Probabilistic Model and Analysis. *Biophys. J.* **1990**, *58*, 841–856.
19. Cozens-Roberts, C.; Quin, J. A.; Lauffenburger, D. A. Receptor-Mediated Cell Attachment and Detachment Kinetics: II. Experimental Model Studies with the Radial-Flow Detachment Assay. *Biophys. J.* **1990**, *58*, 857–872.
20. Javanmard, M.; Babrzadeh, F.; Davis, R. W. Microfluidic Force Spectroscopy for Characterization of Bimolecular Interactions with Piconewton Resolution. *App. Phys. Lett.* **2010**, *97*, 173704.
21. Javanmard, M.; Emaminerjad, S.; Dutton, R. W.; Davis, R. W. Use of Negative Dielectrophoresis for Selective Elution of Protein-Bound Particles. *Anal. Chem.* **2012**, *84*, 1432–1438.
22. Yang, Y.; Erb, R. M.; Wiley, B. J.; Zauscher, S.; Yellen, B. B. Imaginary Magnetic Tweezers for Massively Parallel Surface Adhesion Spectroscopy. *Nano Lett.* **2011**, *11*, 1681–1684.
23. Neuman, K. C.; Nagy, A. Single-Molecule Force Spectroscopy; Optical Tweezers, Magnetic Tweezers and Atomic Force Microscopy. *Nat. Methods* **2008**, *5*, 491–505.

24. de Vries, A. H. B.; Krenn, B. E.; Driel, R. V.; Kanger, J. S. Micro Magnetic Tweezers for Nanomanipulation inside Live Cells. *Biophys. J.* **2005**, *88*, 2137–2144.
25. Lee, S. W.; Li, H.; Bashir, R. Dielectrophoretic Tweezers for Examining Particle-Surface Interactions within Microfluidic Devices. *App. Phys. Lett.* **2007**, *90*, 223902–223904.
26. Baek, S. H.; Chang, W.-J.; Baek, J.-Y.; Yoon, D. S.; Bashir, R.; Lee, S. W. Dielectrophoretic Technique for Measurement of Chemical and Biological Interactions. *Anal. Chem.* **2009**, *81*, 7737–7742.
27. Wang, L.; Flanagan, L. A.; Jeon, N. L.; Monuki, E.; Lee, A. P. Dielectrophoresis Switching with Vertical Sidewall Electrodes for Microfluidic Flow Cytometry. *Lab Chip* **2007**, *7*, 1114–1120.
28. Lee, S. W.; Chang, W.-J.; Bashir, R.; Goo, Y.-M. Bottom-up Approach for Implementing Nano/Microstructure Using Biological and Chemical Interactions. *Biotech. Bioprog. Eng.* **2007**, *12*, 185–199.
29. Noy, A.; Frisbie, C. D.; Rozsnayi, L. F.; Wrighton, M. S.; Lieber, C. M. Chemical Force Microscopy: Exploting Chemically-Modified Tips to Quantify Adhesion, Friction, and Functional Group Distributions in Molecular Assemblies. *J. Am. Chem. Soc.* **1995**, *117*, 7943–7951.
30. Papastavrou, G.; Akari, S.; Mohwald, H. Interactions Between Hydrophilic and Hydrophobic Surface on Microscopic Scale and the Influence of Air Bubbles As Observed by Scanning Force Microscopy in Aqueous and Alcoholic Mediums. *Europhys. Lett.* **2002**, *52*, 551–556.
31. Mckendry, R.; Theoclitou, M. E.; Abell, C.; Rayment, T. Role of Surface Perfection in Chemical Force Microscopy. *Langmuir* **1998**, *14*, 2846–2849.
32. Williams, J. M.; Han, T.; Beebe, T. P., Jr. Determination of Single-Bond Forces from Contact Force Variances in Atomic Force Microscopy. *Langmuir* **1996**, *12*, 1291–1295.
33. Williams, P. M. Analytical Descriptions of Dynamic Force Spectroscopy: Behavior of Multiple Connections. *Analy. Chim. Acta* **2003**, *479*, 107–115.
34. Vegte, E. W.; Hanziioannou, G. Scanning Force Microscopy with Chemical Specificity: An Extensive Study of Chemical Specific Tip-Surface Interactions and Chemical Imaging of Surface Functional Groups. *Langmuir* **1997**, *13*, 4357–4368.
35. Han, T.; Williams, J. M.; Beebe, T. P., Jr. Chemical Bonds Studied with Functionalized Atomic Force Microscopy Tips. *Anal. Chim. Acta* **1995**, *307*, 365–376.
36. Guillot, M.; Rchard-Plouet, M.; Vilminot, S. Structural Characterizations of a Lamellar Organic-Inorganic Nickel Silicate Obtained by Hydrothermal Synthesis from Nickel Acetate and (Aminopropyl)triethoxysilane. *J. Mater. Chem.* **2002**, *12*, 851–857.
37. http://www.chemie.fu-berlin.de/chemistry/bio/aminoacid/lysin_en.html.
38. Fu, S.; Li, D.; Luch, C. A. Prediction of Electrophoretic Mobilities. Part 2.+ Effect of Acid Dissociation Constant on the Intrinsic Mobilities of Aliphatic Carboxylates Abd Amines. *Analyst* **1998**, *123*, 1487–1492.
39. Liu, Y.-J.; Guo, S.-S.; Zhang, Z.-L.; Huang, W.-H.; Baigl, D.; Xie, M.; Chen, Y.; Pang, D.-W. A Micropillar-Intergrated Smart Microfluidic Device for Specific Capture and Sorting of Cells. *Electrophoresis* **2007**, *28*, 4713–4722.
40. Koo, O. K.; Liu, Y.; Shuaib, S.; Bhattacharya, S.; Ladisch, M. R.; Bashir, R.; Bhunia, A. K. Targeted Capture of Pathogentic Bacteria Using a Mammalian Cell Receptor Coupled with Dielectrophoretis on a Biochip. *Anal. Chem.* **2009**, *81*, 3094–3101.
41. Leckband, D. E.; Schmitt, F.-J.; Israelachvili, J. N.; Knool, W. Direct Force Measurements of Specific and Non-specific Protein Interaction. *Biochemistry* **1994**, *33*, 4611–4624.
42. Yuan, C.; Chen, A.; Kolb, P.; Moy, V. T. Energy Landscape of Streptavidin-Biotin Complexes Measured by Atomic Force Microscopy. *Biochemistry* **2000**, *39*, 10219–10223.
43. Merkel, R.; Nassoy, P.; Leung, A.; Ritchie, K.; Evans, E. Energy Landscapes of Receptor-Ligand Bonds Explored with Dynamic Force Spectroscopy. *Nature* **1999**, *397*, 50–53.
44. Israelachvili, J.; Pashley, R. M. Measurement of the Hydrophobic Interaction between Two Hydrophobic Surfaces in Aqueous Electrolyte Solutions. *J. Colloid Interface Sci.* **1984**, *98*, 500–514.
45. Gady, B.; Schleef, D.; Reifenberger, R.; Rimai, D.; DeMejo, L. P. Identification of Electrostatic and Van Der Waals Interaction Forces between a Micrometer-Size Particle and a Flat Substrate. *Phys. Rev. B* **1996**, *53*, 8065–8070.